Effect of Rim Thickness on Gear Crack Propagation Path

D. G. Lewicki

Vehicle Propulsion Directorate,
U.S. Army Research Laboratory,
NASA Lewis Research Center,
Cleveland, OH

R. Ballarini

Department of Civil Engineering and
Mechanical & Aerospace Engineering,
Case Western Reserve University,
Cleveland, OH

Analytical and experimental studies were performed to investigate the effect of rim thickness on gear tooth crack propagation. The goal was to determine whether cracks grew through gear teeth or through gear rims for various rim thicknesses. A finite element based computer program (FRANC, FRacture ANalysis Code) simulated gear tooth crack propagation. The analysis used principles of linear elastic fracture mechanics. Quarter-point, triangular elements were used at the crack tip to represent the stress singularity. The program had an automated crack propagation option in which cracks were grown numerically using an automated re-meshing scheme. Crack tip stress intensity factors were estimated to determine crack propagation direction. Gears with various backup ratios (rim thickness divided by tooth height) were tested to validate crack path predictions. Gear bending fatigue tests were performed in a spur gear fatigue rig. From both predictions and tests, gears with backup ratios of 3.3 and 1.0 produced tooth fractures while a backup ratio of 0.3 produced rim fractures. For a backup ratio of 0.5, the experiments produced rim fractures and the predictions produced both rim and tooth fractures, depending on the initial geometry of the crack.

Introduction

A common design goal for gears in helicopter or turboprop power transmissions is to reduce weight. To help meet this goal, some gear designs use thin rims. Rims that are too thin, however, may lead to bending fatigue problems. Depending on the geometry and load on the gear or the severity of the defect, a crack may propagate through a tooth or into the rim. In aircraft applications, a crack which propagates through a rim would be catastrophic. This could lead to disengagement of a rotor or propeller from an engine, loss of an aircraft, and fatalities. This type of failure mode should be avoided. On the other hand, a crack which propagates through a tooth may or may not be catastrophic. The severity of this failure mode would depend on design conditions (such as contact ratio) and whether the debris remained in mesh to jam the gear train. Also, ample warning of this failure mode may be possible due to advances in modern diagnostic systems.

Proper tooth design can usually prevent gear tooth bending fatigue. However, gear tooth or rim fatigue failures may occur even when the tooth design itself is adequate. Possible causes of such failures are insufficient rim thickness in the design, improperly processed material containing inclusions where cracks can start, severe operating conditions such as overload or misalignment, operation near the resonant frequency of a gear structure, or localized wear such as fretting at a gear-shaft connecting joint which could initiate a crack (McFadden, 1985; Albrecht, 1988; Couchan et al., 1993).

The most common methods of gear design and analysis are based on standards published by the American Gear Manufacturers Association. Included in the standards are rating formulas for gear tooth bending to prevent crack initiation (AGMA, 1990). These standards can include the effect of rim thickness on tooth bending fatigue (Drago and Lutthans, 1983). The standards, however, do not give any indication of the crack propagation path once a crack has started. In fact, no gear analysis design tool currently exists which can predict whether a crack will propagate through a tooth or through the rim.

Fracture mechanics has developed into a useful discipline for predicting strength and life of cracked structures. Only a handful of references, however, are available in which fracture mechanics was applied to gear tooth bending fatigue problems. Among the earliest, Ahmad and Loo (1977) applied fracture mechanics to gear teeth to illustrate the procedure and estimate crack propagation direction. Honda and Conway (1979) also applied fracture mechanics to simulate tooth crack propagation, compute threshold loads, and calculate tooth life. Flasker and Jezernik (1983) applied fracture mechanics to gear teeth to estimate stress intensity factors and gear life. Researchers at Tohoku University in Japan performed a series of analyses and experiments to determine the effect of residual stress on crack initiation and propagation (Kato et al., 1990; Inoue et al., 1991). Flasker and Pehan (1993) described their method for calculating crack propagation in gear teeth using fracture mechanics. Danie-wicz (1994) developed a comprehensive, self-contained analysis package to refine the spur gear bending fatigue theory using fracture mechanics. Lastly, Nicoletto (1993) and Abersek and Flasker (1994) described their approaches to estimate stress intensity factors for cracked gear teeth using the weight function method. Much of the work of the above references considered only an initial crack and propagation paths were not considered. Many of the references that did consider crack propagation assumed the propagation occurred in a straight path. In addition, experimental validation of the cited analyses was sparse. Finally, no work using fracture mechanics was performed for thin-rim gears.

The objective of this study was to determine the effect of gear rim thickness on crack propagation path. The major emphasis was to predict the direction in which a crack will grow, either through the gear tooth or through the rim. Linear elastic fracture analysis was used to analyze gear tooth bending fatigue in standard and thin-rim gears. Finite element computer programs were used to determine stress distributions and model crack propagation. Experimental tests were performed to validate predicted crack propagation results.

Analysis

Fundamentals of Fracture Mechanics. Modern-day fracture mechanics has become a powerful tool for analysis of cracked structures (Anderson, 1991). Consider three types of loading on a cracked body: mode I, mode II, and mode III. For mode I, the load is applied normal to the crack plane and tends

to open the crack. Mode II refers to in-plane shear loading or sliding. Mode III corresponds to out-of-plane loading or tearing. Linear elastic fracture mechanics, as the name implies, is based on a linear elastic material with no plastic deformation. Williams (1957) demonstrated that the stress distribution and displacement field ahead of a crack tip in an isotropic linear elastic material can be written as

$$\sigma_{ij} = \frac{1}{\sqrt{2\pi r}} [K_I f^I_{ij}(\theta) + K_{II} f^{II}_{ij}(\theta) + K_{III} f^{III}_{ij}(\theta)] \quad (1)$$

$$u_i = \frac{1}{\mu} \sqrt{\frac{r}{2\pi}} [K_I g^I_i(\theta) + K_{II} g^{II}_i(\theta) + K_{III} g^{III}_i(\theta)] \quad (2)$$

where σ_{ij} are the components of the stress tensor, u_i are the displacements, r and θ are position coordinates (Fig. 1), K_I, K_{II}, and K_{III} are the stress intensity factors for modes I, II, and III, respectively, μ is the shear modulus, and f^I_{ij}, f^{II}_{ij}, f^{III}_{ij}, g^I_i, g^{II}_i, and g^{III}_i are known universal functions. For the current study, the analysis was simplified to a two-dimensional problem and considered only mode I and mode II loading.

From Eq. (1), the stress ahead of the crack tip can be described by the stress intensity factor. The stress intensity factor is a function of geometry and load. A number of methods can be used to estimate the stress intensity factor such as Green's functions, weight functions, boundary integral equations, finite element method (FEM), or experimental techniques. For other than simple geometry and loading, closed-form solutions for the stress intensity factor are not available and methods such as FEM or experiments are used. With the growing capacities of computers today FEM techniques have become extremely popular.

Also from EQ. (1), the stress distribution near the crack tip exhibits a $1/\sqrt{r}$ singularity. When using the FEM technique with conventional finite elements, a large number of elements near the crack tip is required for high accuracy (Chan et al., 1970). Work by Henshell and Shaw (1975) and Barsoum (1976) overcame this deficiency. Here, standard six-node triangular elements were used, with the mid-side nodes on sides adjacent to the crack tip moved from the nominal mid-position to one-quarter of the length (Fig. 2). It was shown by these studies that this type of mesh modeled the inverse square-root singularity of stress distribution near a crack tip.

The direct output of the finite element method is calculated nodal displacements for which nodal forces, stresses, and strains can be determined. For fracture mechanics, stress intensity factors are of primary interest and can also be estimated based on the nodal displacements and forces. A variety of methods to estimate stress intensity factors have been developed based on the finite element nodal values. One popular method to calculate stress intensity factors is called the displacement correlation method. By correlating the displacement relationship of Eq. (2) with the displacement relationship of the finite element analysis using quarter-node elements, it can be shown (Tracey, 1977)
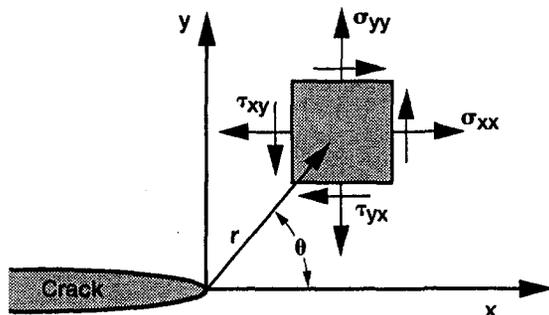
Fig. 2 Quarter-node, isoparametric, six-node triangular, finite elements used for the region near a crack tip

that the stress intensity factors as a function of the nodal displacements are

$$K_I = \frac{\mu}{\kappa + 1} \sqrt{\frac{2\pi}{L}} [4(v_b - v_d) + v_e - v_c] \quad (3)$$

$$K_{II} = \frac{\mu}{\kappa + 1} \sqrt{\frac{2\pi}{L}} [4(u_b - u_d) + u_e - u_c] \quad (4)$$

$$\mu = \frac{E}{2(1 + \nu)} \quad (5)$$

$$\kappa = \begin{cases} 3 - 4\nu & \text{for plane strain} \\ \dfrac{3 - \nu}{1 + \nu} & \text{for plane stress} \end{cases} \quad (6)$$

where E is the modulus of elasticity, ν is Poisson's ratio, L is the element length, and u_i and v_i are nodal displacements in the x and y directions, respectively (Fig. 2).

Once the mode I and II stress intensity factors are known, the predicted crack propagation angle can be estimated under mixed mode loading. The method of Erdogan and Sih (1963) was used which states that the crack extension starts at the crack tip and grows in the radial direction in the plane perpendicular to the direction of the maximum tangential tensile stress. Mathematically, the predicted crack propagation angle can be written as

$$\theta_m = 2 \tan^{-1} \left[\frac{\dfrac{K_I}{K_{II}} \pm \sqrt{\left(\dfrac{K_I}{K_{II}}\right)^2 + 8}}{4} \right] \quad (7)$$

The predicted crack propagation angle is defined relative to the coordinate system shown in Fig. 1 and setting $\theta = \theta_m$. In Fig. 1, θ is shown in the positive sense.

Crack Propagation Simulation. The analysis of this present study used the FRANC (FRacture ANalysis Code) computer program described by Wawrzynek (1991). FRANC is a general purpose finite element code for the static analysis of cracked structures. FRANC is designed for two-dimensional problems and is capable of analyzing plane strain, plane stress, or axisymmetric problems.

Among the variety of capabilities, a unique feature of FRANC is the ability to model a crack in a structure. FRANC uses a method called "delete and fill" to accomplish this. To illustrate the principle, first consider a finite element mesh of

Fig. 1 Coordinate axes ahead of crack tip
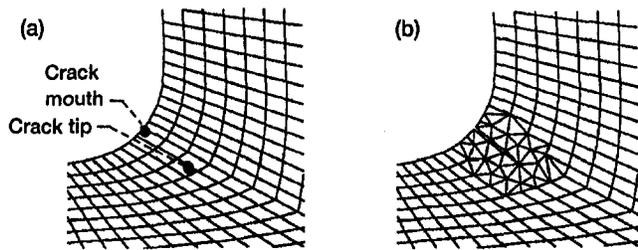
Fig. 3 FRANC computer program crack modeling scheme (a) user defined mouth and tip of initial crack (b) final mesh of cracked surface

an uncracked structure. The user would first define an initial crack by identifying the node of the crack mouth and coordinates of the crack tip (Fig. 3a). FRANC will then delete the elements in the vicinity of the crack tip. Next, FRANC will insert a rosette of quarter-point, six-node triangular elements around the crack tip to model the inverse square-root stress singularity. Finally, FRANC will fill the remaining area between the rosette and original mesh with conventional six-node triangular elements (Fig. 3b). The user can then run the finite element equation solver to determine nodal displacements, forces, stresses, and strains. FRANC can then calculate stress intensity factors using the displacement correlation method and the predicted crack propagation angle using the maximum tangential stress theory.

A further unique feature of FRANC is the automatic crack propagation capability. After an initial crack is inserted in a mesh, FRANC models a propagated crack as a number of straight line segments. For each segment, FRANC models the crack tip using a rosette of quarter-point elements. FRANC then solves the finite element equations, calculates the stress intensity factors, and calculates the crack propagation angle. FRANC then places the new crack tip at the calculated angle and at a user-defined crack increment length. The model is then remeshed using the "delete and fill" method described above. The procedure is repeated a specific number of times as specified by the user. It should be noted that the local $x-y$ coordinate system of Figures 1 and 2 move with the crack tip as crack propagation is numerically simulated.

Gear Modeling. Basic gear tooth geometry data was input to a tooth coordinate generation computer program. The tooth coordinate generator program used the method of Hefeng et al. (1985) to determine the tooth coordinates. The output was tooth coordinate and rim coordinate data which defined a single-tooth sector of a gear. This output was used by a commercially available pre- and post-processing finite element analysis software package (P3/PATRAN, 1993). This package created the finite element mesh of the complete gear. FRANC then used this mesh and performed crack propagation simulations.

Figure 4 shows a sample finite element mesh of an uncracked gear. Table I lists the gear geometry. The tooth geometry used closely matched that of the test gears of the NASA Lewis Spur Gear Fatigue Rig (described in the following section). The analysis used 8-node, plane stress, quadrilateral finite elements. The material used was steel. For boundary conditions, four hub nodes were fixed.

In detailed studies (Lewicki, 1995), a variety of mesh refinement in the region near the insertion of the crack were analyzed to determine the effect of mesh refinement on maximum principal stress in the tooth fillet region. The chosen refinement of Fig. 4 had 2353 elements and 7295 nodes. This refinement, along with the use of the quarter-point elements produced accurate calculations of the stress intensity factors. As a check, the FRANC modeling procedure was used to analyze simple structures where closed-form solutions for the stress intensity factors were known (three point bend specimen and
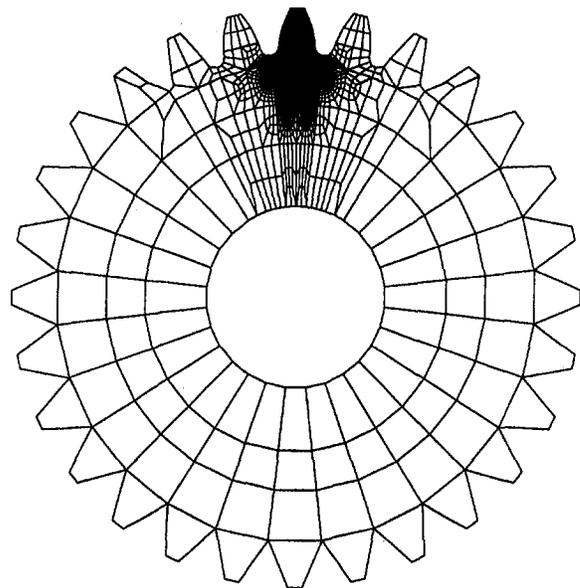
Fig. 4 Finite element model of gear used in crack propagation studies

compact tension specimen). Other checks using the FRANC modeling procedure are also referenced in the literature (Wawrzynek, 1991).

For meshing gears, tooth loads vary in magnitude (due to load sharing) as well as location along the tooth profile. For the present analysis, the tooth load was placed at the location of the highest point of single tooth contact on the cracked tooth. This resulted from a detailed study of the effect of gear tooth load position on predicted crack propagation direction (Lewicki, 1995). The study considered loads at various positions on the crack tooth, loads on the teeth adjacent to the cracked tooth, and load sharing.

The gears that were modeled also included notches in the fillet region to match that of the gears tested (described in the following section). In addition, gears with various rim thicknesses were modeled. The parameter describing the rim thickness was the backup ratio, m_B, where

$$m_B = \frac{b}{h} \qquad (8)$$

where b was the rim thickness, and h was the tooth whole depth. Gears with various backup ratios were modeled by incorporating slots in the model. The slots were incorporated in the model by removing various elements in the rim region of the gear.

Table 1 Test gear geometry (gear tolerance per AGMA class 12)

Number of teeth	28
Module, mm/teeth (diametral pitch, teeth/in.)	3.2 (8)
Circular pitch, mm (in.)	9.98 (0.393)
Whole depth, mm (in.)	7.62 (0.300)
Addendum, mm (in.)	3.20 (0.125)
Chordal tooth thickness, mm (in.)	4.85 (0.191)
Pressure angle, deg	20
Pitch diameter, mm (in.)	88.90 (3.500)
Outside diameter, mm (in.)	95.25 (3.750)
Root fillet, mm (in.)	1.02 to 1.52 (0.040 to 0.060)
Measurement over pins, mm (in.)	96.04 to 96.32 (3.781 to 3.792)
Pin diameter, mm (in.)	5.49 (0.216)
Backlash reference, mm (in.)	0.25 (0.010)
Tip relief at tooth tip, μm (in.)	12.7 (0.0005)
Tooth profile surface finish, μm rms (μin. rms)	0.41 (16)
Tooth and rim width, mm (in.)	6.35 (0.250)
Hub width, mm (in.)	19.05 (0.750)
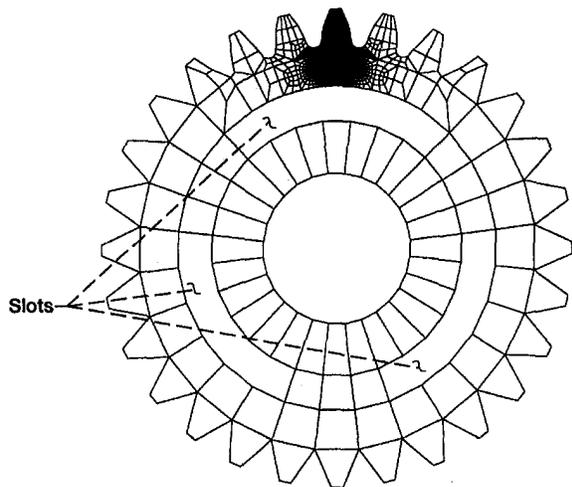
Fig. 5 Finite element mesh of slotted gear used in crack propagation studies of thin-rim gears, $m_B = 1.0$

Figure 5 shows a sample mesh for $m_B = 1.0$. By using slots to emulate various rim thicknesses, the models for the various rim thicknesses used the same mesh refinement for the loaded tooth.

Experiments

Test Facility. Crack propagation experiments were performed in the NASA Lewis Spur Gear Fatigue Rig (Fig. 6). The test stand operated on a torque-regenerative principle in which torque was circulated in a loop of test gears and slave gears. Oil pressure was supplied to load vanes in one slave gear which displaced the gear with respect to its shaft. This produced a torque on the test gears, slave gears, and connecting shafts proportional to the amount of applied oil pressure. An 18.6-kW (25-hp), variable-speed motor provided speed to the drive shaft using a belt and pulley. Note that in a torque-regenerative system, the required input drive power needs only to overcome the frictional losses in the system.

Separate lubrication systems were provided for the tests gears and the main gearbox. The test gears were lubricated using a single oil jet at the in-to-mesh location. The main gearbox lubrication system provided oil to the loading vanes using a high-pressure pump. Also, the main gearbox lubrication system provided oil to the slave gears and support bearings. The test gear and main gearbox lubrication systems were separated by labyrinth seals on the gear shafts pressurized with nitrogen gas. Even though two separate systems existed, a common oil was used for both since some leakage occurred between the two. The lubricant used was a synthetic paraffinic oil. In addition, the test gear lubricant was filtered through a 5-micron fiberglass filter.

The NASA Lewis Spur Gear Fatigue Rig was primarily developed for surface pitting fatigue life investigations. For surface pitting fatigue tests, the test gears are run offset to increase the tooth contact stress and promote surface fatigue. For the current crack propagation studies, however, the desired failure mode was tooth bending fatigue. Therefore, the gears were run full contact, not offset.

Test Gears. The test gear geometry data are given in Table 1. The gears were external spur gears. The teeth had involute profiles with linear tip relief starting at the highest point of single tooth contact and ending at the tooth tip. The maximum amount of tip relief was 0.013 mm (0.0005 in.) at the tooth tip.

All gears used in the experiments were fabricated and machined from a single batch of material. The test gear material was consumable-electrode vacuum-melted AISI 9310 steel. The

gears were case-carburized and ground. The teeth were hardened to a case hardness of R_c 61 and a core hardness of R_c 38. The effective case depth (depth at a hardness of R_c 50) was 0.81 mm (0.032 in.). To determine the effect of rim thickness on crack propagation, slots were machined in some gears to emulate various rim thicknesses. Backup ratios of $m_B = 3.3$ (no slots), 1.0, 0.5, and 0.3 were tested (Fig. 7). By using slots in this manner, the same tooth geometry was used in all cases and thus, not a variable in the study.

It was believed that tooth bending fatigue cracks would be difficult to initiate based on the load capacity of the test rig. Due to this limitation, notches were fabricated in the fillet region (loaded side) on one tooth of each of the test gears to promote crack initiation. Table 2 gives the notch dimensions of the test gears used in the experiments. Figure 8 shows a magnified view of a typical notched tooth. The notches were fabricated using electrodischarge machining (EDM) with a 0.10-mm (0.004-in.) diameter wire electrode. The measured notch dimensions ranged from lengths of 0.13 to 0.33 mm (0.005 to 0.013 in.), widths from 0.10 to 0.23 mm (0.004 to 0.009 in.), and machined along the entire tooth face width. The notches were located at the same location for all the gears. This location was at a radius of 40.49 mm (1.594 in.) on the fillet which was the position of the greatest tensile stress for the solid gear ($m_B = 3.3$). The notches produced a stress concentration factor of approximately three as determined using a finite element analysis.

Instrumentation and Test Procedure. The standard test rig instrumentation monitored test gear speed, oil load pressure, test gear and slave gear oil pressure, and oil temperatures. Also, overall test stand vibration was monitored using an accelerometer mounted on the top housing. In addition to the standard facility vibration sensor, an advanced vibration processing diagnostic system was installed in the test stand to help assist in crack detection.

The objective of the tests was to determine the effect of rim thickness on gear crack propagation direction. The results would then be used to validate the analytical predictions. Eight tests were performed and the corresponding test gear serial numbers (S/N's) are given in Table 2. The notched gears were the driver gears of the test pair. Unmodified gears fabricated from the same batch of material as the notched gears were used as the driven gears.

The test procedure for all tests was the same. The gears were run at 10,000 rpm for all tests. At the start of each test, all gears were initially run at 10.9 N·m (96 in·lb) applied torque for
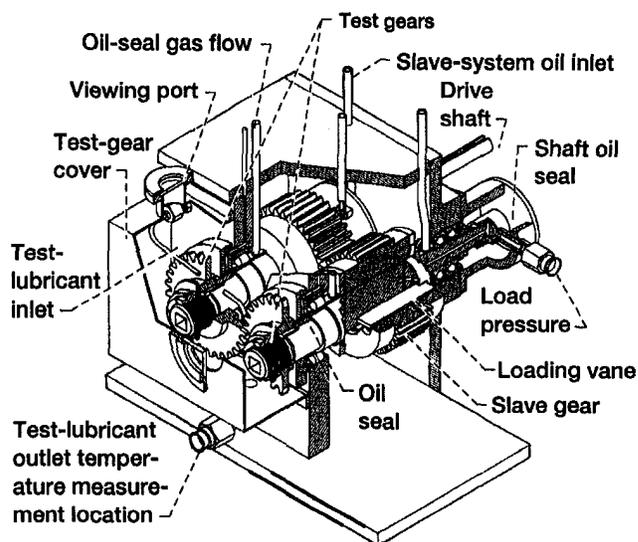
Fig. 6 NASA Lewis spur gear fatigue rig
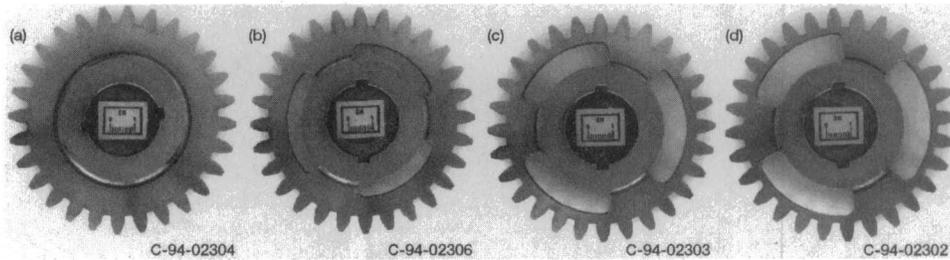
Fig. 7 Various backup ratios used in tests to determine effect of rim thickness on crack propagation (a) m_B = 3.3 (b) m_B = 1.0 (c) m_B = 0.5 (d) m_B = 0.3

one hour as a break-in procedure. After break-in, the load was set for the required test conditions. These conditions ranged from 26.4 to 143.4 N·m torque (234 to 1269 in·lb), depending on the test. After reaching the desired load pressure, a strip chart recorder monitoring oil temperatures was turned on along with the vibration processing system. The gears were run at a steady load condition until failure occurred or a different load level was desired. Test gear oil inlet temperature was 39°C (102°F). Test gear oil outlet temperature was stable and a function of applied torque. As an example, the oil outlet temperature was 60°C (140°F) at 26.4 N·m (234 in·lb) load and 79°C (175°F) at 143.4 N·m (1269 in·lb) load. After occurrence of a failure (tooth or rim breakage), the gears were removed from the rig, cleaned, and photographed.

Results and Discussion

Predicted Crack Paths. Models of the eight gears tested in the Spur Gear Fatigue Rig were analyzed using the finite element method. A stress analysis was first performed without any cracks introduced in the models. Table 3 lists the calculated principal stresses with and without the notches for the uncracked gears.

When notches were not considered, the maximum principal stress (maximum tensile stress) occurred on the fillet surface of the tooth on the loaded side. As the backup ratio decreased from m_B = 3.3 to m_B = 0.5, the magnitude of the maximum principal stress slightly decreased. This was due to the increased compliance of the rim structure as the rim thickness decreased. At m_B = 0.3, however, the magnitude of the maximum principal stress significantly increased. This was due to an inadequate amount of rim material which was needed to support the loaded tooth. For $0.5 \leq m_B \leq 3.3$, the location of the maximum principal stress was at 30 deg $\leq \psi \leq$ 36 deg (see Table 3 for the definition of ψ). At m_B = 0.3, the location of the maximum principal stress moved toward the root of the tooth to ψ = 63°.

When notches were considered in the models, the stress concentration factors were functions of notch length, notch width, and backup ratio, and ranged from 2.41 to 3.38. This analysis was based on the notch dimensions given in Table 2. For S/

N's 01 through 07, the stress concentration factors were fairly consistent with an average value of 3.2. The stress concentration factor for S/N 08 was significantly lower than the others due to a larger notch width. In all cases, the location of the maximum principal stress was at the tip of the notch.

The notches did not affect the stress distribution on the unloaded side of the tooth (location of minimum principal stress which was the maximum compressive stress). The magnitude of the minimum principal stress increased as m_B decreased. Also, the location of the minimum principal stress moved toward the root of the tooth as m_B decreased.

Next, FRANC was used to simulate crack propagation for test gears S/N 01 through 08. The finite element models with notches as previously described were used. For all cases, the mouths of the initial cracks were placed at the nodes located at the tip of the notches. This was the location of the maximum tensile stress. This was also the location of the crack initiation from the experiments. The lengths of the initial cracks were all set equal to 0.25 mm (0.01 in.) and at the same orientations as the notches.

The mode I and II stress intensity factors for the simulated crack propagation of test gears S/N 01 through 08 are shown in Fig. 9. The mode I stress intensity factors gradually increased with increasing crack length, indicating unstable crack growth with constant load. In addition, the mode II stress intensity factor played an important role in crack propagation. For cases of $m_B \geq 1.0$ (Figs. 10a and 10b), the mode II stress intensity factors were negative, which produced positive crack propagation angles (relative to the $x-y$ coordinate axes of Fig. 1). This lead to a crack trajectory which produced tooth fracture. For cases of m_B = 0.3 (Fig. 10d), the mode II stress intensity factors were positive for crack lengths greater than 0.25 mm, which produced negative crack propagation angles. This lead to crack propagation through the gear rim which should be avoided in

Table 2 Notch dimensions of test gears

Serial number, S/N	Backup ratio, m_B	Notch dimensions	
		Length, mm (in.)	Width, mm (in.)
01	3.3	0.15 (0.006)	0.18 (0.007)
02	3.3	0.28 (0.011)	0.15 (0.006)
03	1.0	0.30 (0.012)	0.15 (0.006)
04	1.0	0.13 (0.005)	0.10 (0.004)
05	0.5	0.25 (0.010)	0.20 (0.008)
06	0.5	0.25 (0.010)	0.18 (0.007)
07	0.3	0.33 (0.013)	0.10 (0.004)
08	0.3	0.23 (0.009)	0.23 (0.009)
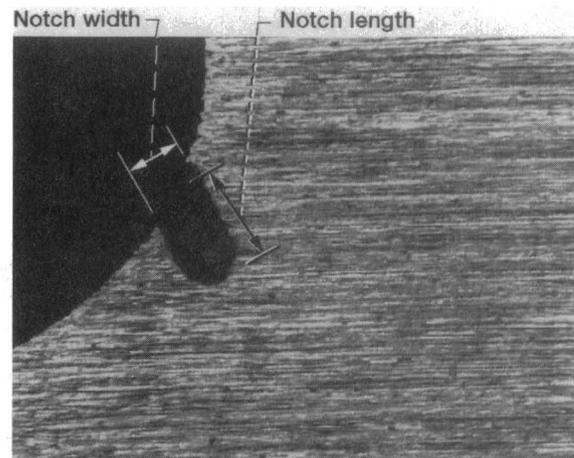
Fig. 8 Magnified view of fabricated notch in tooth fillet region of test gears to promote crack initiation

Table 3 Calculated principal stresses for finite element models of test gears S/N 01 through 08

S/N	m_B	Maximum principal stress				Min prin stress	
		Without notch		With notch		Stress, MPa	Ψ, deg
		Stress, MPa	Ψ, deg	Stress,* MPa	Stress conc factor		
01	3.3	291	36	861	2.96	351	30
02	3.3	291	36	957	3.29	351	30
03	1.0	268	30	880	3.28	399	42
04	1.0	268	30	862	3.22	399	42
05	0.5	243	36	738	3.04	603	57
06	0.5	243	36	763	3.14	603	57
07	0.3	361	63	1222	3.39	1029	63
08	0.3	361	63	870	2.41	1029	63

*Location of maximum principal stress at notch tip for all cases.

the design of a gear set. The case of $m_B = 0.5$ (Figure 10c) was the transition point where predicted crack propagation was somewhere between tooth fracture and rim fracture. Note the only difference between the models of similar backup ratios were notch dimensions, and thus, initial crack locations. That is, the model for gear S/N 01 was the same as that for S/N 02 except for the notch, S/N 03 was same as S/N 04 except for the notch, and so on. The differences were rather minor and the

calculated stress intensity factors and predicted crack propagation paths for identical backup ratios were nearly the same.

To gain further understanding of the effect of rim thickness on crack propagation direction, an analysis was performed in which the orientation of the initial crack was varied in the models of $m_B = 3.3, 0.5,$ and 0.3 (Fig. 11). For $m_B = 3.3$, the crack propagated through the tooth, not the rim, for all orientation angles of the initial crack. Conversely, the crack propagated through the rim for all crack angle orientations of $m_B = 0.3$. The predicted crack propagation path for $m_B = 0.5$, however, was unstable. For a 0, 30, and 60 deg initial crack, the crack propagated through the tooth. For 90 deg, the crack propagated

O S/N 01, mB = 3.3 △ S/N 05, mB = 0.5
● S/N 02, mB = 3.3 ▲ S/N 06, mB = 0.5
□ S/N 03, mB = 1.0 ✳ S/N 07, mB = 0.3
■ S/N 04, mB = 1.0 ✦ S/N 08, mB = 0.3
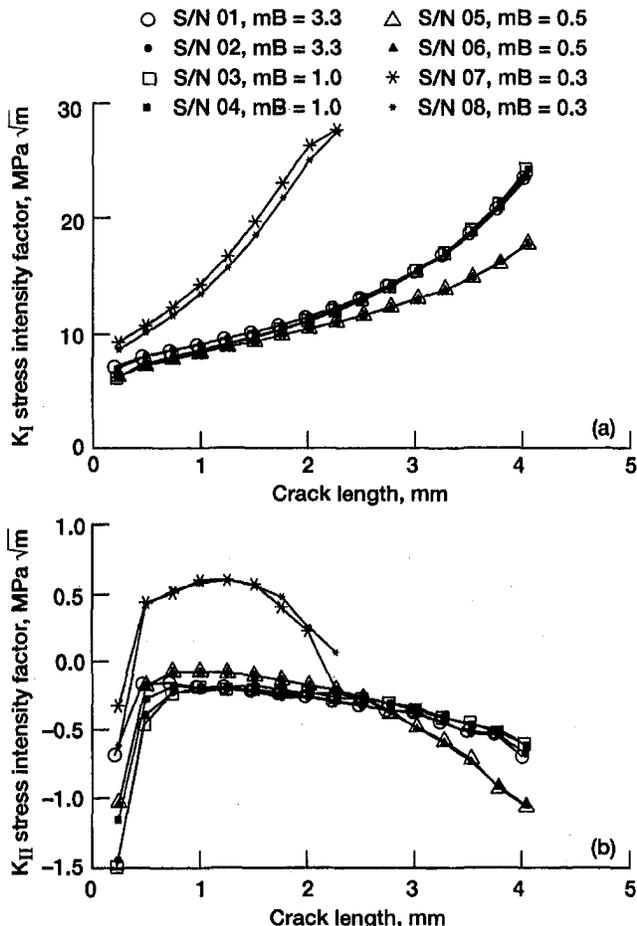
Fig. 9 Calculated stress intensity factors for test gears S/N 01 through 08 (a) Mode I stress intensity factors (b) Mode II stress intensity factors
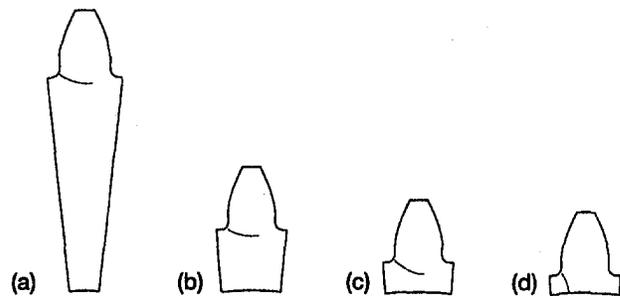
Fig. 10 Predicted crack propagation paths for test gears S/N 01 through 08 (a) S/N 01 and S/N 02, $m_B = 3.3$ (b) S/N 03 and S/N, 04 $m_B = 1.0$ (c) S/N 05 and S/N 06, $m_B = 0.5$ (d) S/N 07 and S/N 08, $m_B = 0.3$

Initial crack, deg
1 0
2 30
3 60
4 90
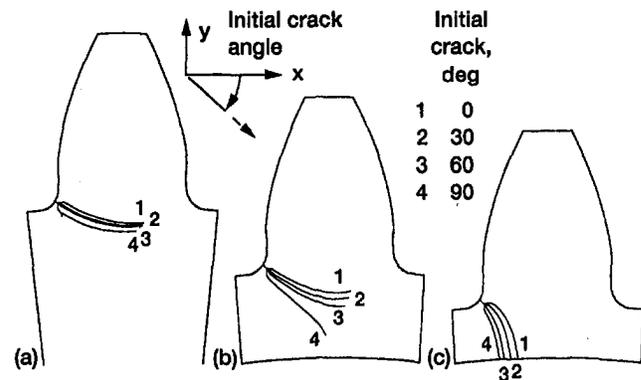
Fig. 11 Effect of initial crack orientation on predicted crack propagation path (a) S/N 01, $m_B = 3.3$ (b) S/N 05, $m_B = 0.5$ (c) S/N 07, $m_B = 0.3$

through the rim. Thus, the case of $m_B = 0.5$ for these studies was the transition point. For $m_B > 0.5$, the crack propagated through the tooth. For $m_B < 0.5$, the crack propagated through the rim. For $m_B = 0.5$, the crack path was unstable and depended on the initial conditions. Other parameters such as small perturbations in rim thickness as well as tooth load position also significantly affected the crack path for the $m_B = 0.5$ transition case.

Experimental Results. Eight tests were performed corresponding to the eight test gears of Table II. For the first two tests, the load was gradually increased in step increments as the run progressed. It was desired to run the tests at the lightest possible load that would still produce crack initiation. This was desired to minimize rig wear (bearings and splines), retard crack propagation once it started (to avoid rapid fracture), and for general safety concerns since tooth or rim fractures were the failure modes. For test 1 (S/N 01, $m_B = 3.3$), the test was run for 4.2 hr. at 26.4 N·m (96 in·lb) torque, 2.8 hr. at 73.2 N·m (648 in·lb), and 0.4 hr. at 143.4 N·m (1269 in·lb) (maximum load available from rig). Tooth fracture (Fig. 12a) occurred at 8.4 hr. total run time and at 143.4 N·m (1269 in·lb) torque. Fracture originated at the tip of the fabricated notch and propagated through only the tooth and not the gear rim. The fracture occurred uniformly throughout the gear tooth face width. For test 2 (S/N 02, $m_B = 3.3$), the gears were run at 73.2 N·m (648 in·lb) torque for 9.0 hr., 88.8 N·m (786 in·lb) for 7.0 hr., 104.4 N·m (924 in·lb) for 7.0 hr., and 120.0 N·m (1062 in·lb) for 3.4 hr. Fracture occurred at 27.4 hr., originated at the notch tip, and propagated through the tooth uniformly throughout the tooth face width.
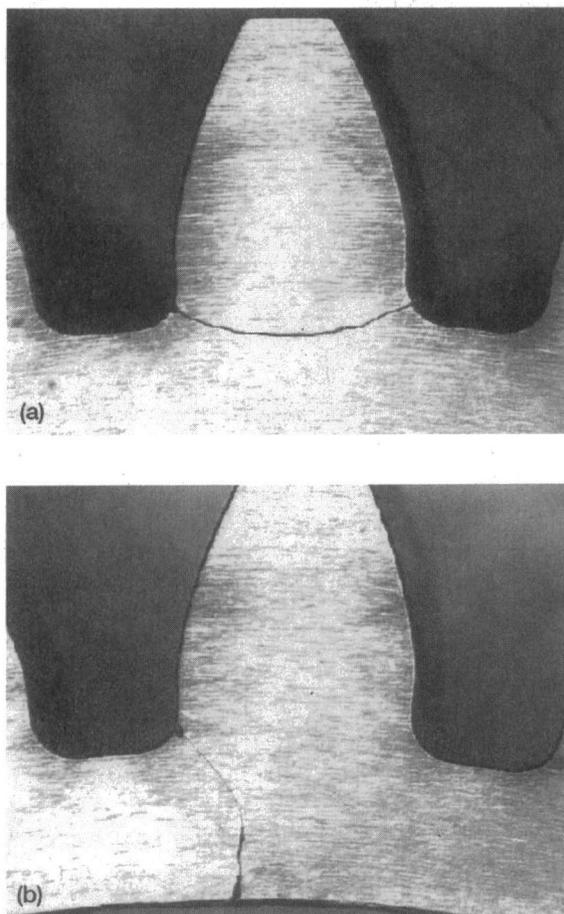
Fig. 12 Sample crack propagation path for tests (a) Test 1, S/N 01, m_B = 3.3, tooth fracture at 8.4 hr total run time (b) Test 5, S/N 05, m_B = 0.5, rim fracture at 5.4 hr total run time
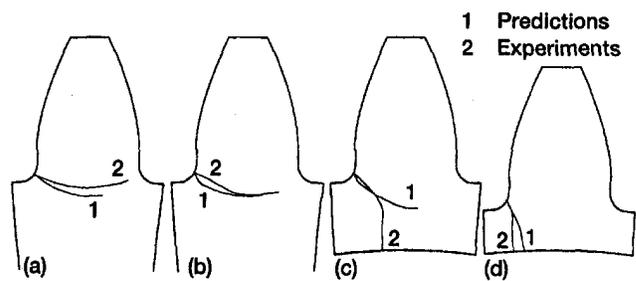
Fig. 13 Comparison of predicted and experimental crack propagation paths for test gears S/N 01 through 08 (a) S/N 01, m_B = 3.3 (b) S/N 03, m_B = 1.0 (c) S/N 05, m_B = 0.5 (d) S/N 07, m_B = 0.3

Based on the experience of tests 1 and 2, the majority of the remaining tests were run at 120.0 N·m (1062 in·lb) torque. For test 3 (S/N 03, $m_B = 1.0$), the gears were run at 120.0 N·m (1062 in·lb) for a total of 3.9 hr. Again, tooth fracture occurred, originating at the fabricated notch, and propagated through the tooth. Test 4 (S/N 04, $m_B = 1.0$) was also run at 120.0 N·m (1062 in·lb) but was inconclusive. At 22.9 hr. total run time, no crack initiation occurred and the test was suspended.

Test 5 (S/N 05, $m_B = 0.5$) was run at 120.0 N·m (1062 in·lb) torque and was concluded after 5.4 hr. total run time. At 5.4 hr., a crack originated at the fabricated notch, propagated in a straight path for a short distance, then turned direction and propagated through the gear rim (Fig. 12b). Test 6 (S/N 06, $m_B = 0.5$) was run at 120.0 N·m (1062 in·lb) torque for 27.0 hr. and then 143.4 N·m (1269 in·lb) for 0.9 hr. At this time, rim failure occurred. A crack started at the fabricated notch and propagated through the rim similar to test 5. In addition, secondary rim damage occurred due to the high dynamic loads caused by the rim failure. The rim was broken in two pieces as a result. Test 7 (S/N 07, $m_B = 0.3$) ended after only 9 min. of testing at 120.0 N·m (1062 in·lb) torque. A crack started at the notch and propagated directly through the rim. Test 8 (S/N 08, $m_B = 0.3$) was run at only 88.8 N·m (786 in·lb) torque due to the sudden failure of test 7. After 3.8 hr. at this load, rim fracture occurred similar to test 7.

Comparison of Crack Path Predictions to Experiments. The predicted crack propagation paths for the models of the test gears are shown in Fig. 13. Also shown for comparison are the results of the experiments. For backup ratios $m_B \geq 1.0$, the cracks propagated through the teeth and the correlation between predicted crack paths and experiments was rather good (Figs. 13a and 13b). For the other extreme of $m_B = 0.3$, the cracks propagated through the rim, and again, the correlation between predictions and experiments was good (Fig. 13d). A discrepancy occurred for the $m_B = 0.5$ cases (Fig. 13c). The predicted crack paths for these cases propagated in a fairly straight path with a slight tendency back toward the tooth. The crack paths from the experiments, however, propagated through the rims.

As was previously addressed, the predictions for the $m_B = 0.5$ case was unstable and the crack paths were dependent on initial conditions. Various conditions such as initial crack angles, load positions, or small perturbations of the backup ratio affected the stress field in the tooth and rim region enough to significantly alter crack path direction. It is obvious from Fig. 13c that the stress fields of the gears during testing were slightly different than that modeled since the predicted crack paths diverged from the experimental results. It was not known exactly what these differences were. One possibility could have been residual stress fields in the test gears due to the fabrication of the slots or residual stress due to the carburization process. Another possibility could have been slight deviations in the model and notch dimensions and initial crack locations compared to the test gears due to measurement errors. Overall,

considering all cases modeled and tested, the predictions correlated well with the experiments. Care and conservatism should be used, however, when modeling thin-rim gears where the transition from tooth failure to rim failure occurs.

Conclusions

Analytical and experimental studies were performed to investigate the effect of rim thickness on gear tooth crack propagation. A major emphasis was to determine the direction in which cracks grew, through the teeth or through the rims. Gear tooth crack propagation was simulated using a finite element based computer program which used principles of linear elastic fracture mechanics. Crack tip stress intensity factors were estimated and used to determine crack propagation direction. In addition to the analysis, experimental studies were performed in the NASA Lewis Spur Gear Fatigue Rig. Gears with various backup ratios were tested to validate crack path predictions. The following conclusions were made:

1) For backup ratios (defined as rim thickness divided by tooth height) of $m_B = 3.3$ and 1.0, the analysis predicted cracks that would propagate through the teeth and not the rims. This was validated by the experiments.

2) For $m_B = 0.3$, the analysis predicted cracks that would propagate through the rim, which was also validated by experiments.

3) For $m_B = 0.5$, the experiments produced rim fractures while the analysis showed instability (tooth or rim fracture) when various initial conditions were changed. The analytical results at the transition point of tooth to rim failure should be viewed with conservatism to produce a safe gear design.

Acknowledgment

References

Abersek, B., and Flasker, J., 1994, "Stress Intensity Factor for Cracked Gear Tooth," *Theoretical and Applied Fracture Mechanics*, Vol. 20, pp. 99–104.

AGMA, 1990, "Fundamental Rating Factors and Calculation Methods for Involute Spur and Helical Gear Teeth," ANSI/AGMA 2001-B88, American Gear Manufacturers Association, Alexandria, VA.

Ahmad, J., and Loo, F. T., 1977, "On the Use of Strain Energy Density Fracture Criterion in the Design of Gears Using Finite Element Method," ASME Paper No. 77-DET-158, presented at the Design Technical Conference, Chicago, IL, Jun.

Albrecht, C., 1988, "Transmission Design Using Finite Element Method Analysis Techniques," *Journal of American Helicopter Society*, Vol. 33, No. 2, Apr., pp 3–14.

Anderson, T. L., 1991, *Fracture Mechanics—Fundamentals and Applications*, CRC Press, Boca Raton, Florida.

Barsoum, R. S., 1976, "On the Use of Isoparametric Finite Elements in Linear Fracture Mechanics," *International Journal for Numerical Methods in Engineering*, Vol. 10, No. 1, pp. 25–37.

Chan, S. K., Tuba, I. S., and Wilson, W. K., 1970, "On the Finite Element Method in Linear Fracture Mechanics," *Engineering Fracture Mechanics*, Vol. 2, No. 1-A, pp. 1–17.

Couchan, D. C., Barnes, G. K., and Cedoz, R. W., 1993, "Shot-Peened Gear Failures Due to Operation in a Misaligned Condition," AIAA Paper No. AIAA-93-2147, presented at the 29th Joint Propulsion Conference, Monterey, CA, Jun.

Daniewicz, S. R., Collins, J. A., and Houser, D. R., 1994, "The Stress Intensity Factor and Stiffness for a Cracked Spur Gear Tooth," ASME JOURNAL OF MECHANICAL DESIGN, Vol. 116, No. 3, pp. 697–700.

Drago, R. J., and Lutthans, R. V., 1983, "Combined Effects of Rim Thickness and Pitch Diameter on Spur Gear Tooth Stresses," *Journal of the American Helicopter Society*, Vol. 28, Jul., pp 13–19.

Erdogan, F., and Sih, G. C., 1963, "On the Crack Extension in Plates Under Plane Loading and Transverse Shear," *Journal of Basic Engineering*, Vol. 85, pp. 519–527.

Flasker, J., and Jezernik, A., 1983, "The Comparative Analysis of Crack Propagation in the Gear Tooth," *Proceedings of the International Conference of Application of Fracture Mechanics to Materials and Structures*, Freiburg, West Germany, Jun., pp. 971–982.

Flasker, J., and Pehan, S., 1993, "Crack Propagation in Tooth Root With Variable Loading," *Communications in Numerical Methods in Engineering*, Vol. 9, No. 2, Feb., pp. 103–110.

Hefeng, B., Savage, M., and Knorr, R. J., 1985, "Computer Modeling of Rack-Generated Spur Gears," *Mechanism and Machine Theory*, Vol. 20, No. 4, pp. 351–360.

Henshell, R. D., and Shaw, K. G., 1975, "Crack Tip Finite Elements Are Unnecessary," *International Journal for Numerical Methods in Engineering*, Vol. 9, pp. 495–507.

Honda, H., and Conway, J. C., 1979, "An Analysis by Finite Element Techniques of the Effects of a Crack in the Gear Tooth Fillet and its Applicability to Evaluating Strength of the Flawed Gears," *Bulletin of the JSME*, Vol. 22, No. 174, Dec., pp. 1848–1855.

Inoue, K., Kato, M., Deng, G., and Takatsu, N., 1991, "Fracture Mechanics Based Evaluation of Strength of Carburized Gear Teeth," *Proceedings of the JSME International Conference on Motion and Power Transmissions*, Hiroshima, Japan, Nov., pp. 801–806.

Kato, M., Inoue, K., Deng, G., and Jeong, B. S., 1990, "Strength Evaluation of Carburized Gear Teeth Based on Fracture Mechanics," *Proceedings of the KSME/JSME Joint Conference, Fracture and Strength '90*, Seoul, Korea, pp. 248–253.

Lewicki, D. G., 1995, "Crack Propagation Studies to Determine Benign or Catastrophic Failure Modes for Aerospace Thin-Rim Gears," Ph.D. Dissertation, Case Western Reserve University.

McFadden, P. D., 1985, "Analysis of the Vibration of the Input Bevel Pinion in RAN Wessex Helicopter Main Rotor Gearbox WAK143 Prior To Failure," Aeronautical Research Laboratories Report No. AR-004-049.

Nicoletto, G., 1993, "Approximate Stress Intensity Factors for Cracked Gear Teeth," *Engineering Fracture Mechanics*, Vol. 44, No. 2, pp. 231–242.

P3/PATRAN, 1993, P3/PATRAN User Manual, PDA Engineering, Costa Mesa, CA.

Tracey, D. M., 1977, "Discussion of 'On the Use of Isoparametric Finite Elements in Linear Fracture Mechanics' by R. S. Barsoum," *International Journal for Numerical Methods in Engineering*, Vol. 11, pp. 401–402.

Wawrzynek, P. A., 1991, "Discrete Modeling of Crack Propagation: Theoretical Aspects and Implementation Issues in Two and Three Dimensions," Ph.D. Dissertation, Cornell University.

Williams, M. L., 1957, "On the Stress Distribution at the Base of a Stationary Crack," ASME *Journal of Applied Mechanics*, Vol. 24, No. 1, Mar., pp. 109–114.